Cellular/Molecular

Nonlinear [Ca^{2+}] Signaling in Dendrites and Spines Caused by Activity-Dependent Depression of Ca^{2+} Extrusion

Volker Scheuss,[1] Ryohei Yasuda,[1] Aleksander Sobczyk,[1,2] and Karel Svoboda[1]

[1]Howard Hughes Medical Institute, Cold Spring Harbor Laboratory, Cold Spring Harbor, New York 11724, and [2]Department of Physics, State University of New York at Stony Brook, Stony Brook, New York 11794

Spine Ca^{2+} triggers the induction of synaptic plasticity and other adaptive neuronal responses. The amplitude and time course of Ca^{2+} signals specify the activation of the signaling pathways that trigger different forms of plasticity such as long-term potentiation and depression. The shapes of Ca^{2+} signals are determined by the dynamics of Ca^{2+} sources, Ca^{2+} buffers, and Ca^{2+} extrusion mechanisms. Here we show in rat CA1 pyramidal neurons that plasma membrane Ca^{2+} pumps (PMCAs) and Na^+/Ca^{2+} exchangers are the major Ca^{2+} extrusion pathways in spines and small dendrites. Surprisingly, we found that Ca^{2+} extrusion via PMCA and Na^+/Ca^{2+} exchangers slows in an activity-dependent manner, mediated by intracellular Na^+ and Ca^{2+} accumulations. This activity-dependent depression of Ca^{2+} extrusion is, in part, attributable to Ca^{2+}-dependent inactivation of PMCAs. Ca^{2+} extrusion recovers from depression with a time constant of ~0.5 s. Depression of Ca^{2+} extrusion provides a positive feedback loop, converting small differences in stimuli into large differences in Ca^{2+} concentration. Depression of Ca^{2+} extrusion produces Ca^{2+} concentration dynamics that depend on the history of neuronal activity and therefore likely modulates the induction of synaptic plasticity.

Key words: **calcium extrusion; plasma membrane calcium pump; sodium calcium exchanger; dendritic spine; calcium imaging; two-photon glutamate uncaging**

Introduction

Dendritic spines receive the majority of excitatory synapses (Nimchinsky et al., 2002) and contain elaborate signal transduction complexes associated with the postsynaptic density and the actin cytoskeleton (Kennedy, 2000). Spines are diffusionally isolated from their parent dendrites and other spines (Harris and Stevens, 1989; Svoboda et al., 1996; Majewska et al., 2000b; Sabatini and Svoboda, 2000). Local [Ca^{2+}] transients in spines and dendrites activate diverse signal transduction pathways that trigger synapse-specific adaptive neuronal responses, including long-term depression and potentiation (Cummings et al., 1996).

How is specificity in Ca^{2+} signaling achieved? It is likely that the local amplitude and time course of [Ca^{2+}] signals are critical in determining the activation of Ca^{2+}- dependent pathways. These signals are shaped by the spatial organization and kinetics of Ca^{2+} sources, buffers, and extrusion mechanisms (Sabatini et al., 2001). During synaptic activity, Ca^{2+} ions enter spines both through synaptic NMDA receptors (NMDARs) (Muller and Connor, 1991; Murphy et al., 1994; Yuste and Denk, 1995; Koester and Sakmann, 1998; Mainen et al., 1999; Kovalchuk et al., 2000) and voltage-sensitive calcium channels (VSCCs) (Schiller et al., 1998). Under some conditions, Ca^{2+} may also enter the spine cytosol via Ca^{2+}-induced Ca^{2+} release (CICR) (Emptage et al., 1999).

In CA1 pyramidal neurons, action potentials (APs) propagate into proximal dendrites and open VSCCs, leading to relatively global [Ca^{2+}] elevations in spines and dendrites (Callaway and Ross, 1995; Yuste and Denk, 1995; Sabatini and Svoboda, 2000). Because APs produce essentially instantaneous and global Ca^{2+} influx, the resulting [Ca^{2+}] signals are straightforward to interpret and have thus been used to study Ca^{2+} handling in dendrites and spines (Helmchen et al., 1996; Lee et al., 2000; Maravall et al., 2000; Sabatini and Svoboda, 2000; Sabatini et al., 2002).

Ca^{2+} ions are rapidly extruded (~10 ms) from the cytoplasm of CA1 spines (Sabatini et al., 2002), but little is known about the extrusion mechanisms. Uptake into intracellular stores via smooth endoplasmic reticulum Ca^{2+}-ATPase (SERCA) pumps seems to account for only a small fraction of extrusion in a subpopulation of hippocampal spines (Sabatini et al., 2002). Other mechanisms are likely to be more important, including plasma membrane Ca^{2+} pumps (PMCAs) and Na^+/Ca^{2+} exchangers (NCX, NCKX) (Blaustein and Lederer, 1999; Strehler and Zacharias, 2001; Kiedrowski, 2004).

Using [Ca^{2+}] imaging, we show that both PMCAs and Na^+/Ca^{2+} exchangers contribute to extrusion from spines. Unexpectedly, extrusion slows in an activity- and Ca^{2+}-dependent manner, providing a mechanism for positive feedback in [Ca^{2+}] signaling. Depression of extrusion leads to spike-timing-

Received March 17, 2006; revised June 21, 2006; accepted June 21, 2006.

This work was supported by NYSTAR (New York State Office of Science, Technology, and Academic Research), the National Institutes of Health, the Howard Hughes Medical Institute, the Human Frontiers Science Program (V.S.), the Burroughs Wellcome Fund, and the Dana Foundation (R.Y.). We thank Karen Zito and Richard Weinberg for critical reading of this manuscript.

Correspondence should be addressed to Dr. Karel Svoboda, Howard Hughes Medical Institute, Janelia Farm Research Campus, 19700 Helix Drive, Ashburn, VA 20147.

V. Scheuss' present address: Howard Hughes Medical Institute, Janelia Farm Research Campus, 19700 Helix Drive, Ashburn, VA 20147.

R. Yasuda's present address: Neurobiology Department, Duke University Medical Center, Durham, NC 27710.

DOI:10.1523/JNEUROSCI.1962-06.2006

 0270-6474/06/268183-12$15.00/0

dependent plasticity (STDP) of $[Ca^{2+}]$ signals in dendritic spines. This novel mechanism may play a role in translating differences in neuronal activity into differential activation of Ca^{2+}-dependent signaling pathways to trigger different forms of synaptic plasticity such as long-term potentiation and depression.

Materials and Methods

Electrophysiology. Acute transverse hippocampal slices (300 μm thick) were prepared from 16- to 20-d-old Sprague Dawley rats in chilled dissection solution (in mM: 110 choline chloride, 25 $NaHCO_3$, 25 D-glucose, 11.6 Na-ascorbate, 7 $MgCl_2$, 3.1 Na-pyruvate. 2.5 KCl, 1.25 NaH_2PO_4, 0.5 $CaCl_2$) as described previously (Sabatini et al., 2002) and in accordance with the animal care and use guidelines of Cold Spring Harbor Laboratory. Slices were incubated in artificial CSF (ACSF) (in mM: 127 $NaCl_2$, 25 $NaHCO_3$, 25 D-glucose, 2.5 KCl, 1 $MgCl_2$, 2 $CaCl_2$, 1.25 NaH_2PO_4) bubbled with carbogen (95% O_2, 5% CO_2) at 35°C for 30–60 min and further at room temperature until use. In the recording chamber, the extracellular solution was ACSF bubbled with carbogen at 35°C. Somatic whole-cell recordings (pipette resistance, 3–5 MΩ) were performed on visually identified CA1 pyramidal neurons. Data were acquired via an Axopatch 200B patch amplifier controlled with custom software written in Matlab (The Mathworks, Natick, MA). For recordings in current-clamp mode, the internal solution contained (in mM) 135 K-methylsulfonate, 10 HEPES, 10 Na-phosphocreatine, 4 $MgCl_2$, 4 Na-ATP, and 0.4 Na-GTP and, in addition, 30 μM Alexa-594 and one of the Ca^{2+} indicators, Fluo-4FF (500 μM) or Fluo-4 (500 μM) (Molecular Probes, Eugene, OR), for imaging. Ca^{2+} influx was induced with back-propagating APs evoked by somatic current injection (1–2 nA, 2–3 ms). Stimulation protocols were repeated every 10 s and consisted of a single AP, followed (Fluo4FF, after 500 ms; Fluo-4, after 1500 ms) by trains of APs with alternating frequencies (20, 50, or 80 Hz). For recordings in voltage-clamp mode, $CsMeSO_4$ replaced K-methylsulfonate in the internal solution. Drugs were from Sigma (St. Louis, MO), unless stated otherwise. Calmidazolium (Calbiochem, La Jolla, CA) was dissolved in DMSO (final concentration, 0.13%). When NaCl (127 mM) in the ACSF was replaced with an equimolar amount of LiCl, some Na^+ (25 mM) remained in the modified ACSF from the drugs necessary for the carbonate pH-buffer system. However, because the intracellular pipette solution contained 14.4 mM Na^+, the Na^+ concentration gradient across the plasma membrane is effectively abolished.

Imaging. Two-photon laser-scanning microscopy was performed with a custom microscope (objective: 60×, 0.9 numerical aperture; Olympus, Tokyo, Japan) (Yasuda et al., 2004). The light source was a Ti:Sapphire laser (Mira; Coherent, Santa Clara, CA) running at lamda ~810 nm. Image acquisition was controlled by ScanImage (Pologruto et al., 2003). Neurons were loaded with indicators for 15–20 min before imaging. Imaged spines were on small secondary or tertiary dendrites close to the soma (<100 μm). This ensured rapid dye equilibration and good electrophysiological control and avoided nonlinearities in Ca^{2+} influx associated with changes in AP waveform during trains of back-propagating APs (Callaway and Ross, 1995). The fluorescence from Alexa-594 [red (R)] and Fluo Ca^{2+} [green (G)] indicators were detected simultaneously in transfluorescence and epifluorescence mode. Fluorescence signals from the spine and parent dendrite were recorded using line scans (500 Hz) that intersect both structures (Fig. 1*A*). To reduce illumination and photodamage, the excitation beam was blanked during the rising phase of $[Ca^{2+}]$ transients (Fig. 1*B*,*D*) using a Pockels Cell (Con Optics, Dansbury, CT). During each acquisition, the dark current of the photomultipliers was recorded before shutter opening and subtracted from the fluorescence signals.

The intensity profile along the line scans in the red channel ($[Ca^{2+}]$-insensitive) signal (Fig. 1*B*, top, right inset) was used to set the regions of interest (ROIs) for the spine and dendrite (fluorescence intensity >70% of the peak). The fluorescence signals were computed by integration over the ROI. The ratio G/R was used as a measure of $[Ca^{2+}]$ (Yasuda et al., 2004). To estimate saturation and absolute Ca^{2+} concentration, we measured G/R at saturating $[Ca^{2+}]$ $[(G/R)_{max}]$. $(G/R)_{max}$ was measured in a patch electrode, containing internal solution with 10 mM $[Ca^{2+}]$, in a

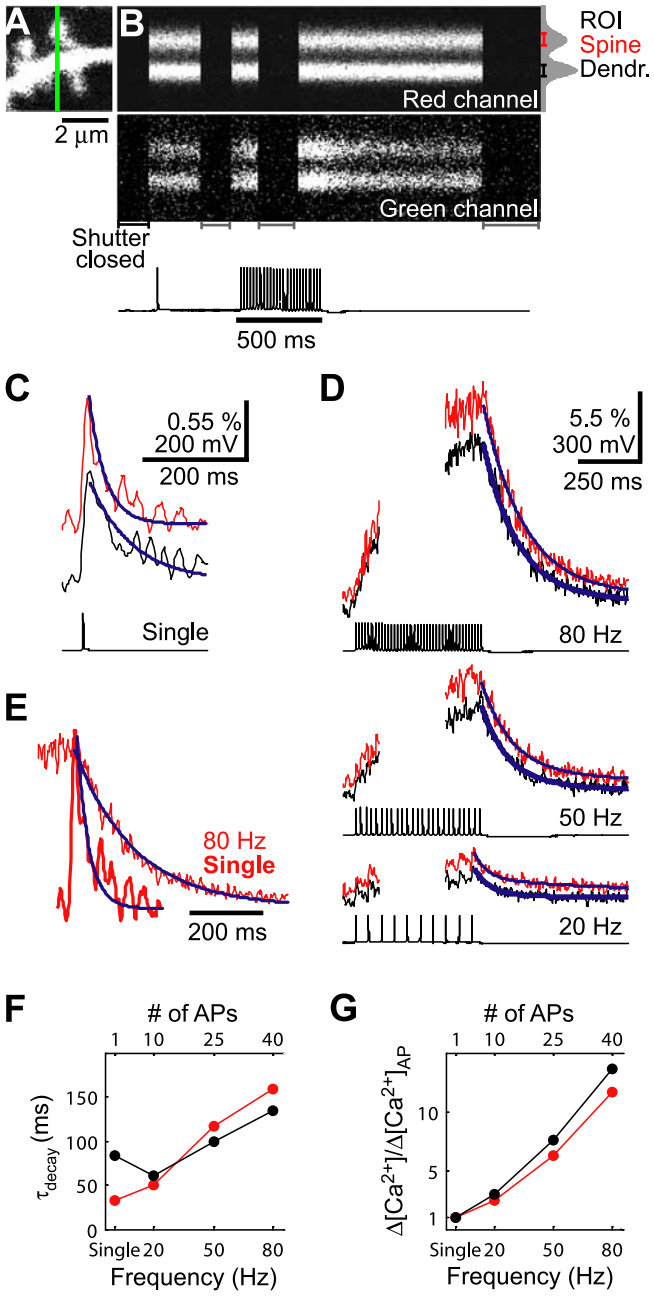

Figure 1. Activity-dependent slowing of the decay of $[Ca^{2+}]$ transients. All panels are from the same experiment. ***A***, Image of a small dendritic branch (red channel). The green line indicates the position of the line scan for rapid $[Ca^{2+}]$ imaging. ***B***, A typical experiment (top, red channel; bottom, green channel). The stimulus was a single AP followed by a train of 25 APs at 50 Hz (average of 10 trials). The fluorescence transient in response to the AP train can be seen in the spine and dendrite (Dendr.) as an increase in fluorescence in the green channel. To minimize photodamage, the excitation light was shuttered during intervals irrelevant for the analysis (shutter closed). Bottom, corresponding membrane voltage trace. ***C***, $[Ca^{2+}]$ transients (top; spine, red; dendrite, black; average of 34 trials) evoked by a single AP (bottom). The traces represent the ratio of green over red fluorescence (G/R) as a fraction of $(G/R)_{max}$ (G/R at saturating $[Ca^{2+}]$) (see Materials and Methods). Blue lines indicate monoexponential fits to determine τ_{decay}. Traces are offset vertically for display. ***D***, $[Ca^{2+}]$ transients evoked by AP trains (top, 80 Hz; middle, 50 Hz; bottom, 20 Hz). Blue lines indicate monoexponential or double-exponential fits to determine τ_{decay} (see Materials and Methods). Traces are offset vertically for display. ***E***, Overlay of the decay phases of peak scaled $[Ca^{2+}]$ transients evoked by a single AP (thick trace) and 80 Hz AP train (thin trace) in the spine. Blue lines indicate exponential fits. ***F***, $[Ca^{2+}]$ transient decay time constants as a function of AP train frequency. ***G***, Normalized $[Ca^{2+}]$ transient peak amplitudes as a function of AP train frequency.

brain slice. To allow comparison of $[Ca^{2+}]$ transient amplitudes recorded with different batches of internal solution, the signals are represented in percentage of $(G/R)_{max}$. To obtain a sufficient signal-to-noise ratio (SNR) for exponential fitting required averaging (20–50 trials for the low-amplitude single AP-evoked signals; 10–20 trials for 20 Hz; 5–10 trials for both 50 and 80 Hz). We restricted analysis to data with stable resting $[Ca^{2+}]$ (G/R) and $[Ca^{2+}]$ transient decay constants in response to trains (<20% change). G/R reports $[Ca^{2+}]$ linearly as long as $[Ca^{2+}] \ll K_D$ (Yasuda et al., 2004). Under our experimental conditions, the effects of dye saturation on measurements of τ_{decay} were <10% (supplemental Fig. 1, available at www.jneurosci.org as supplemental material).

Two-photon glutamate uncaging. For simultaneous two-photon uncaging of glutamate and Ca^{2+} imaging, a second laser beam (720 nm, uncaging beam, Maitai; Spectra Physics, Mountain View, CA) was combined with the imaging beam such that both beams were scanned by the same scan mirrors, but under control of two separate Pockels Cells (Sobczyk et al., 2005). A concentration of 2.5 mM MNI-caged L-glutamate (4-methoxy-7-nitroindolinyl-caged L-glutamate; Tocris, Ellisville, MO), 1 μM thapsigargin, 20 μM ryanodine, 1 μM TTX and, in some experiments, 200 μM MCPG [(*S*)-α-methyl-4-carboxyphenylglycine] and 2 mM ascorbate were added to the ACSF. Mg^{2+} was reduced to 0.1 mM, and experiments were performed in voltage clamp. Precisely timed, local uncaging was achieved by illuminating (50–150 mW in the back-focal plane) next to the spine head during a short segment (0.2 ms) of a single scan line (see Fig. 7*A*).

Analysis. Data were analyzed with custom routines written in Matlab. Decay time constants were determined by fitting mono- or double-exponentials to the decay phase of $[Ca^{2+}]$ transients. Amplitude (single stimuli, peak G/R; trains, mean G/R in 20–50 ms intervals before the last stimulus) and baseline (mean G/R in 20–50 ms intervals before the stimulus) were determined independently and were used to constrain the fit. Transients were considered to decay mono-exponentially if the slow time constant was similar (<10% slower), much longer (>1000×) than the fast time constant, or if the goodness of fit (χ^2) improved <10% with a double-exponential compared with a mono-exponential.

$[Ca^{2+}]$ dynamics in spines and small dendrites is well described by a single-compartment model (Helmchen et al., 1996; Maravall et al., 2000; Sabatini et al., 2002). APs and brief depolarizations evoked virtually an instantaneous, δ-function-like Ca^{2+} influx (Helmchen et al., 1996; Sabatini and Svoboda, 2000). The $[Ca^{2+}]$ transient amplitude is determined by the amount of Ca^{2+} influx. $[Ca^{2+}]$ transients decay exponentially back to baseline with time constant τ_{decay}, directly reflecting the strength of Ca^{2+} extrusion with the extrusion rate constant (Γ). Ca^{2+} buffers such as the Ca^{2+} indicator reduce $[Ca^{2+}]$ transient amplitudes and slow their decay. The amplitude of recorded $[Ca^{2+}]$ transients depends inversely on the total buffer capacity of endogenous buffers (κ_E) and exogenous buffers (κ_B):

$$\Delta[Ca^{2+}] = \frac{\Delta[Ca^{2+}]_{total}}{1 + \kappa_E + \kappa_B}, \quad (1)$$

whereas the decay time constant of $[Ca^{2+}]$ transients is linearly related to the total buffer capacity:

$$\tau_{decay} = \frac{1 + \kappa_E + \kappa_B}{\Gamma}. \quad (2)$$

The exogenous buffer capacity κ_B is given by the incremental Ca^{2+} binding ratio (Neher and Augustine, 1992; Sabatini et al., 2002; Yasuda et al., 2004):

$$\kappa_B = \frac{K_D[B]_{total}}{(K_D + [Ca^{2+}]_0)(K_D + [Ca^{2+}]_0 + \Delta[Ca^{2+}])} \quad (3)$$

where K_D and $[B]_{tot}$ are the affinity and the total concentration of buffer, whereas $[Ca^{2+}]_0$ and $\Delta[Ca^{2+}]$ are basal $[Ca^{2+}]$ and $[Ca^{2+}]$ increments, respectively. In contrast, NMDAR-mediated $[Ca^{2+}]$ signals are more complicated to interpret because NMDAR activation is long (~100 ms), so that Ca^{2+} influx and extrusion overlap in time. Therefore, AP- and depolarization-evoked Ca^{2+} influx is optimal for quantitatively studying the kinetics of Ca^{2+} extrusion in spines and dendrites (Sabatini et al., 2002). Although the single-compartment model may not strictly hold for some of the longer stimulus trains, this is not expected to confound our conclusions, because the dynamics of AP and depolarization-evoked $[Ca^{2+}]$ is similar in spines and small dendrites (Sabatini et al., 2002).

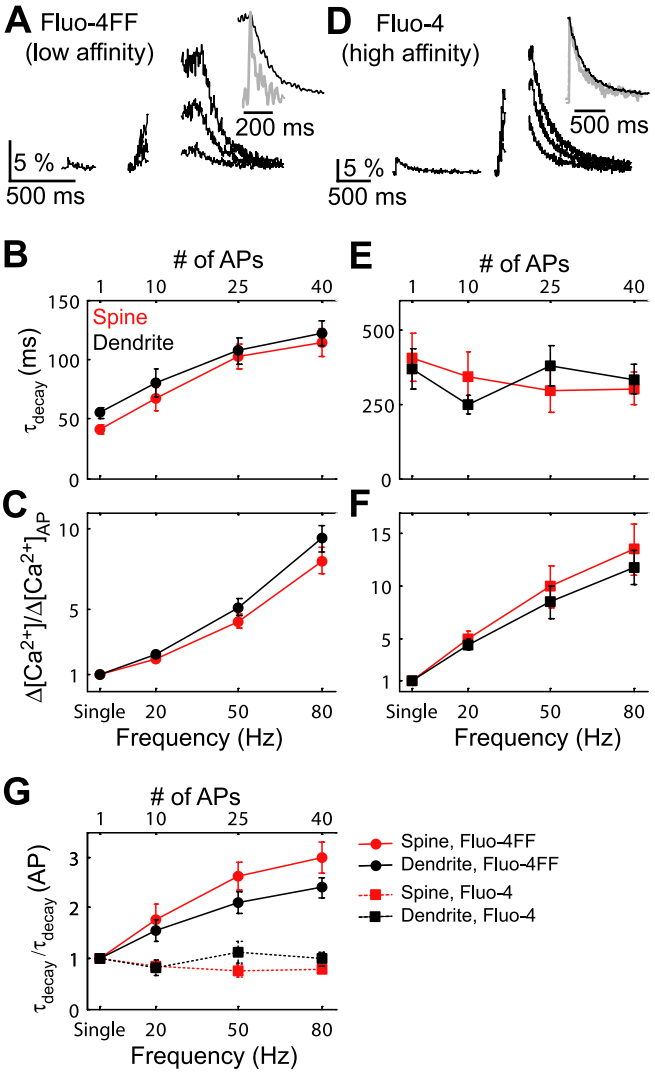

Figure 2. The slowing of the decay of $[Ca^{2+}]$ transients is Ca^{2+} dependent. ***A–C***, Low-affinity Ca^{2+} indicator (Fluo-4FF). ***A***, $[Ca^{2+}]$ transients in a spine (left, single AP; right, AP trains of 20, 50, and 80 Hz). Inset, Overlay of the decay of peak scaled single AP (gray) and 80 Hz AP train (black) evoked $[Ca^{2+}]$ transients. ***B***, $[Ca^{2+}]$ τ_{decay} as a function AP frequency ($n = 17$ cells). ***C***, $[Ca^{2+}]$ transient amplitudes, normalized to the $[Ca^{2+}]$ transient amplitude evoked by single APs (same data set as in ***B***). ***D–F***, High-affinity Ca^{2+} indicator (Fluo-4). ***D***, $[Ca^{2+}]$ transients in a spine (left, single AP; right, AP trains of 20, 50, and 80 Hz). Inset, Overlay of the decay of peak scaled single AP (gray) and 80 Hz AP train (black) evoked $[Ca^{2+}]$ transients. ***E***, $[Ca^{2+}]$ transient decay time constants (τ_{decay}) ($n = 7$ cells). ***F***, $[Ca^{2+}]$ transient amplitudes, normalized to the $[Ca^{2+}]$ transient amplitude evoked by single APs (same data set as in ***E***). ***G***, Normalized decay time constants recorded with Fluo4-FF (solid lines/circles; same data as in ***B***) and Fluo-4 (dashed lines/squares; same data as in ***E***). Error bars indicate SEM.

In hippocampal spines and small dendrites, the reported values are $\kappa_E \approx 20$ nM and $[Ca^{2+}]_0 \approx 70$ nM, and in the absence of exogenous buffer, $\Delta[Ca^{2+}]_{AP}$ is ≈1 μM (Sabatini et al., 2002).

Thus, 500 μM of the low-affinity indicator Fluo-4FF [$K_D = 8.1$ μM at 34°C (Yasuda et al., 2004)] adds a buffer capacity of $\kappa_B \approx 60$. Under our experimental condition, $[Ca^{2+}]$ transients are thus expected to be reduced in amplitude and prolonged in time by a factor of ~4 ($\Delta[Ca^{2+}]_{AP}$, ≈0.25 μM). Over the range of observed $[Ca^{2+}]$ levels (≈0.07–2.5 μM) (Fig. 2*C*), κ_B remains effectively constant because $[Ca^{2+}] \ll K_D$ of Fluo-4FF.

To reduce the $[Ca^{2+}]$ transient amplitudes, we performed some recordings with the high-affinity indicator Fluo-4 (500 μM; $K_D = 0.34$ μM at 34°C) (Yasuda et al., 2004), which adds a buffer capacity of $\kappa_B \approx 1000$ at resting $[Ca^{2+}]$. Thus $[Ca^{2+}]$ transients are expected to be reduced in amplitude and prolonged in time by a factor of ~50 compared with the unbuffered case and by a factor of ~12 compared with our standard recording conditions with Fluo-4FF. K_D values *in situ* can display small deviations from *in vitro* calibrations, and we measure a factor of ~8 difference in τ_{decay} between recordings with Fluo-4FF and Fluo-4 (Fig. 2, compare *B*, *E*).

In experiments with Fluo-4, the expected $[Ca^{2+}]$ levels were ~0.07–0.3 μM (Fig. 2*F*) ($\Delta[Ca^{2+}]_{AP}$, ≈0.02 μM). Because this $[Ca^{2+}]$ range approaches the K_D of Fluo-4, the buffer is partially saturated during trains of APs. Partial saturation reduces the buffer capacity κ_B. Although κ_B is therefore not constant during the decay of a $[Ca^{2+}]$ transient back to baseline, simulations of $[Ca^{2+}]$ transient decays show that this introduces <10% error in estimating the extrusion rate constant Γ from monoexponential fits to the transient decay (supplemental Fig. 1, available at www.jneurosci.org as supplemental material).

During a stimulus train, the plateau, or steady-state level of $[Ca^{2+}]$ above resting $[Ca^{2+}]$, is reached when Ca^{2+} influx and extrusion are balanced:

$$\Delta[Ca^{2+}]_{plateau} = \Delta[Ca^{2+}]_{AP}\tau\upsilon_{AP}, \quad (4)$$

where $\Delta[Ca^{2+}]_{AP}$ is the $[Ca^{2+}]$ increment per AP, τ is the $[Ca^{2+}]$ transient decay time constant, and υ_{AP} is the AP frequency [Helmchen et al. (1996), their Eq. 9]. Because the time integrals of $[Ca^{2+}]$ can be affected by indicator saturation, traces were routinely corrected before integration using the equation $(G/R)_{corr} = (G/R)/(1 - (G/R)/(G/R)_{max})$. The difference in corrected versus uncorrected parameters was <10% in the majority of cases.

In the case of NMDAR-mediated $[Ca^{2+}]$ signals in spines, τ_{decay} does not simply reflect extrusion (Eq. 2) but is also shaped by the time course of the uncaging EPSC (uEPSC) and Ca^{2+} diffusion from the spine head into the dendrite (supplemental Eqs. S9, S10, available at www.jneurosci.org as supplemental material). Therefore, to detect differences in the effectiveness of Ca^{2+} extrusion, we compared the integral of $[Ca^{2+}]$ transients (supplemental Eq. S11, available at www.jneurosci.org as supplemental material). To account for potential differences in the amount of Ca^{2+} influx, we normalized $[Ca^{2+}]$ integrals to the integral of the NMDAR-mediated current.

Averaged data are reported as mean ± SEM. Unless stated otherwise, *n* refers to the number of recorded cells. Statistical significance was evaluated using the paired two-tailed Student's *t* test, unless an unpaired *t* test is indicated. The critical level of significance was $p < 0.05$.

Results

Activity and Ca^{2+} accumulations slow the decay of $[Ca^{2+}]$ transients

Together with Ca^{2+} influx and buffering, Ca^{2+} extrusion is an important determinant of the time course of cytosolic Ca^{2+} signals, especially during the temporal integration resulting from repetitive activity. To study the kinetics of Ca^{2+} extrusion from dendritic spines, we evoked Ca^{2+} influx through VSCCs by firing single back-propagating APs or trains of APs and recorded the resulting $[Ca^{2+}]$ transients in spines and their parent dendrites using two-photon excitation laser-scanning microscopy (Fig. 1*A*,*B*). In contrast to activation of other sources of Ca^{2+}, such as NMDARs, APs cause virtually an instantaneous, δ-function-like Ca^{2+} influx (Helmchen et al., 1996; Maravall et al., 2000; Sabatini et al., 2002). In the absence of continuing influx, the decay of AP-evoked $[Ca^{2+}]$ transients directly reflects the clearance of Ca^{2+} ions from the cytosol. Thus, the decay time constants of the $[Ca^{2+}]$ transients directly reflect the rate of Ca^{2+} extrusion.

Quantitative studies of the mechanisms shaping $[Ca^{2+}]$ signals using $[Ca^{2+}]$ imaging demand conditions that minimize the perturbation of $[Ca^{2+}]$ dynamics by addition of the Ca^{2+} indicator (Neher and Augustine, 1992; Tank et al., 1995; Yasuda et al., 2004). We thus loaded CA1 pyramidal neurons in acute hippocampal brain slices with the low-affinity Ca^{2+} indicator Fluo-4ff ($K_D = 8.1$ μM). To ensure a linear relationship between $[Ca^{2+}]$ and fluorescence, we included relatively high concentrations of the indicator (500 μM). Compared with the unbuffered case, the buffer capacity of the indicator is expected to reduce $[Ca^{2+}]$ transient amplitudes and prolong their durations by a factor of ~4 (Eqs. 1, 2). To visualize neuronal morphology and improve the SNR in $[Ca^{2+}]$ imaging, we also included a red Ca^{2+}-insensitive fluorophore (Alexa 594; 30 μM) (Fig. 1*A*) (Yasuda et al., 2004).

To quantify the rates of Ca^{2+} extrusion, we determined the decay time constants of the $[Ca^{2+}]$ transients (Eq. 2) (Fig. 1*F*) by fitting exponentials to their decay phase (Fig. 1*C–E*, blue lines) (for details, see Materials and Methods). The decay of $[Ca^{2+}]$ transients evoked by single APs was mono-exponential [τ_{decay}(AP); spines, 41 ± 4 ms; dendrites, 55 ± 5 ms; $n = 17$] (Figs. 1*C*,*F*, 2*B*). Taking into account the presence of the indicator, these time constants are consistent with reported values (Sabatini et al., 2002). AP trains evoked larger $[Ca^{2+}]$ transients that decayed with two time constants, a major fast component (<150 ms) followed by a minor slow component (in approximately seconds) (Fig. 1*D*). Surprisingly, the decay time constant of the fast component increased with AP frequency and $[Ca^{2+}]$ both in spines (80 Hz, factor of 3.0 ± 0.3; $n = 17$) and dendrites (2.4 ± 0.2) (Figs. 1*E*,*F*, 2*B*,*G*). The time constant of the slow component was independent of AP frequency. Because its amplitude was ~10 times smaller than the fast component under all conditions (data not shown), we restricted further analysis to the fast time constant and refer to it simply as the time constant of decay, τ_{decay}.

The slowing of $[Ca^{2+}]$ transient decays enhanced the temporal summation of Ca^{2+} such that the peak $[Ca^{2+}]$ increased supralinearly with AP frequency (Figs. 1*G*, 2*C*). This effect could play an important role in $[Ca^{2+}]$ signaling by preferentially enhancing $[Ca^{2+}]$ signals evoked by high levels of activity. Under our conditions, the single AP-evoked $[Ca^{2+}]$ transient amplitudes are expected to be ~0.25 μM in spines and ~0.18 μM in dendrites (see Materials and Methods). The $[Ca^{2+}]$ levels at the end of 20, 50, and 80 Hz trains are expected to be ~0.5, 1.1, and 2.0 μM in spines and ~0.4, 0.9, and 1.6 μM in dendrites, respectively (Fig. 2*C*).

To test whether the activity-dependent increase in τ_{decay} is dependent on $[Ca^{2+}]$, we reduced $[Ca^{2+}]$ transient amplitudes by loading neurons with a high-affinity Ca^{2+} indicator [500 μM Fluo-4; $K_D = 0.34$ μM (Yasuda et al., 2004)] (Fig. 2*D–F*). Compared with our standard conditions (Fig. 2*A-C*), τ_{decay} was prolonged by ≈8-fold (Eq. 2) (Fig. 2*E*), and the amplitudes of $[Ca^{2+}]$ transients were reduced by about the same factor (Eq. 1). Under these conditions, τ_{decay} was independent of AP frequency (Fig. 2*D*,*E*,*G*, squares), suggesting that the increase in τ_{decay} requires high-intracellular Ca^{2+} accumulations (>0.3 μM).

Slowing of $[Ca^{2+}]$ transients is attributable to depression of Ca^{2+} extrusion pathways

Several mechanisms could contribute to slow the decay of $[Ca^{2+}]$ transients including the following: (1) Ca^{2+}-dependent increases in Ca^{2+} buffer capacity; (2) continuing release of Ca^{2+} from Ca^{2+} sources activated during AP trains; (3) saturation of Ca^{2+} extrusion mechanisms; and/or (4) depression of Ca^{2+} extrusion

mechanisms. We performed experiments to test each of these possibilities.

Because the rate of Ca^{2+} extrusion is inversely proportional to the total buffer capacity (Eq. 2), Ca^{2+}-dependent increases in the endogenous Ca^{2+} buffer capacity would increase τ_{decay}. Buffers with nonlinear Ca^{2+} binding could produce activity-dependent increases in buffer capacity and prolong the $[Ca^{2+}]$ transient decay time constant. Such increase in buffer capacity would also reduce the amplitudes of $[Ca^{2+}]$ transients by the same factor (Eqs. 1, 2). Because the opposing effects of increasing buffer capacity on the amplitude and τ_{decay} cancel, the plateau level of $[Ca^{2+}]$ transients during AP trains is expected to be independent of buffer capacity (Eq. 4). Slow buffers (equilibration time $>$ τ_{decay}) would progressively load with Ca^{2+} during a train. However, this would only affect the rate at which the plateau level of $[Ca^{2+}]$ transients is reached, not the plateau level itself. After the stimulus, τ_{decay} would be slowed because of unbinding from the buffer.

Therefore, if nonlinear or slow buffers would account for the slowing of τ_{decay}, then the plateau $[Ca^{2+}]$ levels for AP trains should be equal to the expected plateau $[Ca^{2+}]$ levels based on the $[Ca^{2+}]$ increment ($\Delta[Ca^{2+}]_{AP}$) and τ_{decay} produced by single APs (Regehr and Atluri, 1995; Helmchen et al., 1996). However, when recording with low-affinity buffer (Fluo-4FF), the measured plateau levels were larger than expected (Fig. 3*A*,*B*), implying that the increase in τ_{decay} leads to more effective summation of individual $[Ca^{2+}]$ increments per AP. This argues that activity-dependent changes in buffer capacity cannot explain the slowing of τ_{decay}.

When the activity-dependent increase in τ_{decay} is prevented, $[Ca^{2+}]$ should accumulate linearly (Regehr and Atluri, 1995; Helmchen et al., 1996). Consistent with this prediction, in recordings with high-affinity buffer (Fluo-4), the expected and measured plateau $[Ca^{2+}]$ levels matched (supplemental Fig. 2*A*, available at www.jneurosci.org as supplemental material).

The activity-dependent increase in τ_{decay} could also be caused by sources of Ca^{2+}, which continue to release Ca^{2+} after termination of the AP train, such as CICR (Jacobs and Meyer, 1997; Sandler and Barbara, 1999). In the absence of such sources, $[Ca^{2+}]$ plateau levels during AP trains would be determined by the balance between the $[Ca^{2+}]$ increment per AP and the amount of Ca^{2+} extruded during the interstimulus interval (Eq. 4). Calculating plateau $[Ca^{2+}]$ using the slowed τ_{decay} at the end of the train, we find that the measured and expected plateau levels match ($n = 17$) (Fig. 3*C*). Moreover, blocking CICR pharmacologically (1 μM thapsigargin and 20 μM ryanodine) (Garaschuk et al., 1997) did not prevent slowing of τ_{decay} after a 50 Hz train of depolarizations (see results of recordings in voltage clamp below and Fig. 6*A*). We conclude that continuing Ca^{2+} release from delayed Ca^{2+} sources does not contribute to the slowing of $[Ca^{2+}]$ transient decays.

Could a combination of an increase in buffer capacity, which would slow extrusion, together with Ca^{2+} release from internal stores, which would enhance $[Ca^{2+}]$ levels, explain the results? In this case, when internal stores were blocked with thapsigargin and ryanodine, the measured $[Ca^{2+}]$ plateau levels should be predicted by the plateau levels calculated with the fast τ_{decay}, derived from the $[Ca^{2+}]$ transient evoked by a single stimulus (Eq. 4; compare Fig. 3*B*). However, we found that plateau levels were unaffected by blocking stores and were still predicted best by the slow τ_{decay} after trains of stimuli (supplemental Fig. 2*C*, available at www.jneurosci.org as supplemental material). Thus, release from internal stores in combination with increased endogenous buffer capacity does not explain enhanced Ca^{2+} accumulation and slowing of extrusion.

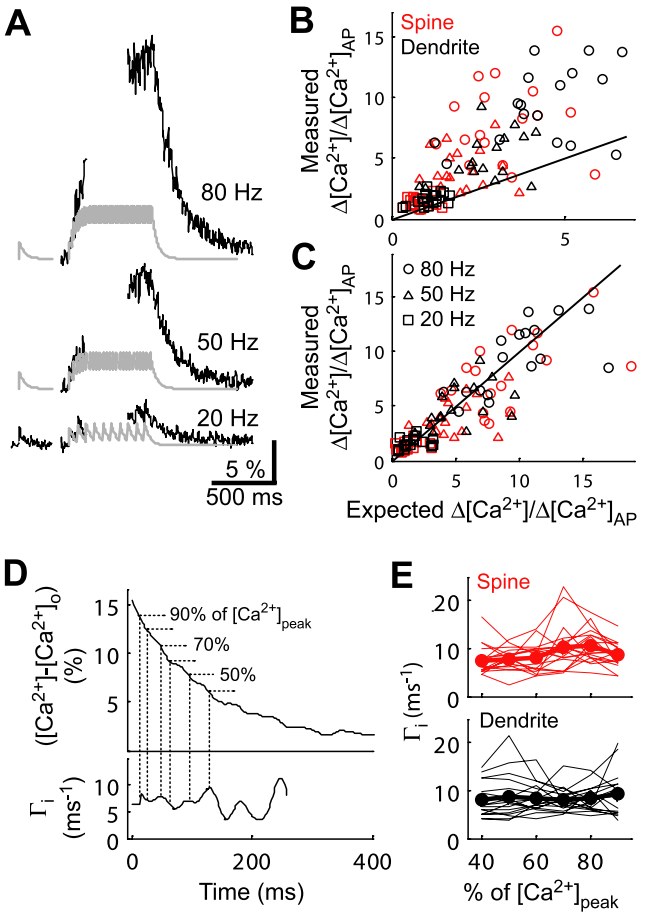

Figure 3. The activity-dependent slowing of the decay of $[Ca^{2+}]$ transients is attributable to depression of Ca^{2+} extrusion mechanisms. ***A***, Comparison of measured $[Ca^{2+}]$ transients (black) and simulated $[Ca^{2+}]$ transients (gray). Simulations were based on the amplitude and decay time of the $[Ca^{2+}]$ transient evoked by a single AP. ***B***, Measured $[Ca^{2+}]$ transient amplitudes versus expected $[Ca^{2+}]$ transient amplitudes, based on the amplitude and decay time of the $[Ca^{2+}]$ transient evoked by a single AP (Eq. 4). The black line shows equality. ***C***, Same as ***B***, except the calculation (Eq. 4) used the decay time of the $[Ca^{2+}]$ transient at the end of AP trains. The black line shows equality. ***D***, Top, The decay phase of a $[Ca^{2+}]$ transient evoked by an 80 Hz AP train in a spine (baseline subtracted). Bottom, Corresponding Γ_i versus time. Dotted lines indicate amplitude levels as a percentage of peak $[Ca^{2+}]$. ***E***, Γ_i versus $[Ca^{2+}]$ level (percentage of peak $[Ca^{2+}]$). To facilitate comparison of the rate constants between cells, instantaneous rate constants were averaged over $[Ca^{2+}]$ level windows of $\pm$10% (thin lines, individual cells; circles, averages; $n = 17$).

These arguments make the assumption that $\Delta[Ca^{2+}]_{AP}$ remains unchanged during trains of APs. This assumption is supported by the observation that the measured $[Ca^{2+}]$ plateau levels and those predicted based on unchanged $\Delta[Ca^{2+}]_{AP}$ match (Fig. 3*C*, Fluo-4FF; supplemental Fig. 2*A*, Fluo-4, available at www.jneurosci.org as supplemental material).

The slowing of Ca^{2+} clearance at high $[Ca^{2+}]$ could also be caused by saturation of Ca^{2+} extrusion mechanisms. At saturation, extrusion mechanisms would operate close to their maximal rate and $[Ca^{2+}]$ transients would decay from their maxima linearly (i.e., with a constant rate). As $[Ca^{2+}]$ drops, the instantaneous rate constant $\Gamma_i = -(d[Ca^{2+}]/dt)/([Ca^{2+}] - [Ca^{2+}]_0)$ would increase with decreasing $[Ca^{2+}]$. As $[Ca^{2+}]$ drops below the $\sim K_D$ of the extrusion mechanism, the decay will become

exponential. Arguing against saturation, we find that Γ_i remains unchanged over the entire range of Ca^{2+} concentrations during the decay of even the largest $[Ca^{2+}]$ transients (Fig. 3*D*,*E*). In addition, $[Ca^{2+}]$ transients of different amplitudes evoked by depolarizations in voltage clamp decayed with the same time constant (see results of recordings in voltage clamp below and Fig. 4*A*–*C*). Thus, saturation of extrusion cannot explain the slowing of $[Ca^{2+}]$ transient decays. Together, these observations argue that the Ca^{2+} accumulations during trains of APs cause a Ca^{2+}-dependent change in the rate constant of extrusion (Eq. 2, Γ). In analogy with previous work on VSCCs (Yasuda et al., 2003), we call this phenomenon depression of Ca^{2+} extrusion.

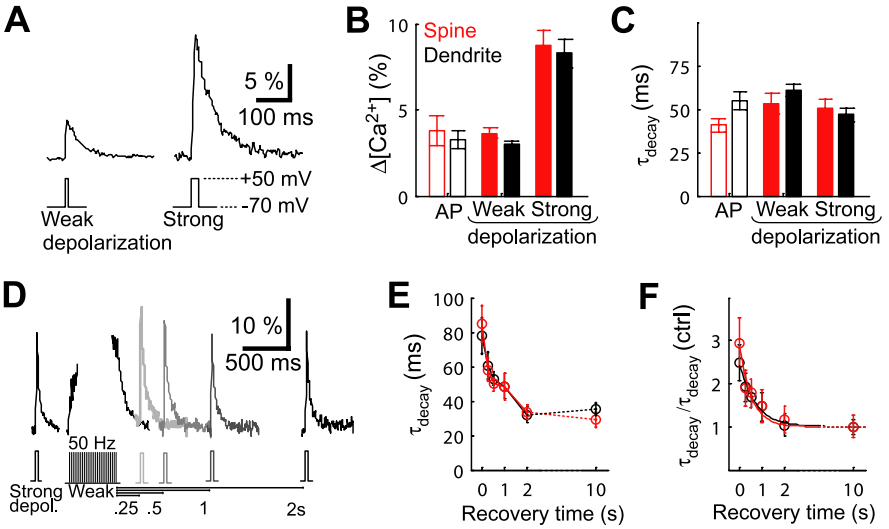

Figure 4. Time constant of the recovery from depression of Ca^{2+} extrusion. ***A***, $[Ca^{2+}]$ transients in a spine evoked by a weak (pulse width, 2–5 ms; left) and a strong (pulse width, 8–15 ms; right) depolarization in voltage clamp. ***B***, Amplitudes of $[Ca^{2+}]$ transients produced by single APs ($n = 5$ cells; open bars) and depolarizations (3–15 ms; $n = 18$ cells; filled bars). ***C***, τ_{decay} of $[Ca^{2+}]$ evoked by APs (open bars; $n = 17$) and depolarizations (filled bars; $n = 18$) (same data set as in ***B***). ***D***, Protocol for measuring the recovery of depression of Ca^{2+} extrusion in a spine. ***E***, Time course of recovery from depression of Ca^{2+} extrusion ($t = 0$; decay time constant of train evoked $[Ca^{2+}]$ transient; $n = 9$). ***F***, Same as ***E***, except normalized with respect to the baseline extrusion time constant. Error bars indicate SEM.

Time constant of recovery from activity-dependent depression of Ca^{2+} extrusion

The activity-dependent slowing of τ_{decay} was not restricted to $[Ca^{2+}]$ transients produced by APs but could also be induced by trains of depolarizations in voltage clamp (Fig. 4). These depolarizations directly activate VSCCs, allowing better experimental control of Ca^{2+} influx and more extensive pharmacological manipulations (e.g., manipulations of ionic gradients that interfere with APs). We therefore used depolarizations produced in voltage clamp in the presence of TTX for a majority of the subsequent experiments while recording $[Ca^{2+}]$ transients with 500 μM Fluo-4FF.

We compared the $[Ca^{2+}]$ transients evoked by depolarizations (Fig. 4*A*–*C*) with those evoked by APs. Applying pulses from a holding potential of −70 to +50 mV induced Ca^{2+} tail currents after repolarization (Sabatini et al., 2002). Varying the pulse width allowed tuning of the fraction of activated channels and the amount of Ca^{2+} influx. Application of single 2–5 ms pulses ("weak" depolarization) mimicked single AP-evoked $[Ca^{2+}]$ transients regarding amplitude and decay time (unpaired *t* test) (Fig. 4*B*,*C*). Larger $[Ca^{2+}]$ transients of about twice the amplitude as obtained with weak depolarization could be evoked using 8–15 ms pulses ("strong" depolarization). τ_{decay} of the $[Ca^{2+}]$ transients evoked by single weak and strong depolarizations and APs were indistinguishable (Fig. 4*C*). Although the amplitude of $[Ca^{2+}]$ transients evoked by strong depolarizations were similar to the amplitude of transients evoked by trains of weak depolarizations (Fig. 4*D*), their duration was not sufficient to induce depression of extrusion. This represents additional evidence that slowing of extrusion is not attributable to saturation of extrusion mechanism. The induction of extrusion depression requires prolonged $[Ca^{2+}]$ elevations.

To analyze the recovery from depression of extrusion, we measured τ_{decay} of $[Ca^{2+}]$ transients evoked by strong depolarizations before and after a 50 Hz train of weak depolarizations and varied the recovery time between the train and the second strong depolarization (Fig. 4*D*). The depression of extrusion recovered with time constants of <1 s (spine, ~500 ms; dendrite, ~700 ms) (Fig. 4*E*,*F*).

Na^+/Ca^{2+} exchangers and PMCAs extrude Ca^{2+} from spines and dendrites

We sought to determine the molecules responsible for Ca^{2+} extrusion in spines and dendrites (Markram et al., 1995; Mainen et al., 1999; Majewska et al., 2000b; Sabatini et al., 2002). In addition to SERCA pumps (Mainen et al., 1999; Majewska et al., 2000b; Sabatini et al., 2002), PMCAs and Na^+/Ca^{2+} exchangers are likely to contribute to extrusion. Both PMCAs and Na^+/Ca^{2+} exchangers derive from multiple genes and occur in multiple splice variants with potentially different properties (Blaustein and Lederer, 1999; Strehler and Zacharias, 2001). Available inhibitors have mostly been tested only on a subset of isoforms and often have nonspecific effects (Kaczorowski et al., 1989; Thayer et al., 2002). We therefore used methods that specifically reduce the activity of Na^+/Ca^{2+} exchangers versus PMCAs, independent of the particular isoform.

PMCAs can be partially inhibited by blocking their activator calmodulin with calmidazolium (Markram et al., 1995; Werth et al., 1996). We recorded $[Ca^{2+}]$ transients evoked by depolarizations before and after wash-in of 20 μM calmidazolium (Fig. 5*A*). Because calmidazolium reduced Ca^{2+} influx (by ~40%), we increased the widths of the depolarizations to keep $[Ca^{2+}]$ transient amplitudes constant (weak depolarizations to 5–10 ms; strong depolarizations to 15–20 ms). Calmidazolium had little effect on resting $[Ca^{2+}]$ in spines and dendrites compared with the amplitudes of depolarization-evoked $[Ca^{2+}]$ transients (relative change in baseline $[Ca^{2+}]$: spine, 0.01 ± 6%; dendrite, 23 ± 4%; transient amplitude relative to baseline $[Ca^{2+}]$: spine, ≈170%; dendrite, ≈90%; $n = 6$) (supplemental Fig. 3*A*,*B*, available at www.jneurosci.org as supplemental material). Because Ca^{2+} influx is effectively instantaneous, quantification of the decay time of $[Ca^{2+}]$ transients isolates the effect of calmidazolium on Ca^{2+} extrusion. Calmidazolium dramatically slowed extrusion for $[Ca^{2+}]$ transients evoked by both weak and strong depolarizations (Fig. 5*B*,*C*). Partial block of PMCA increased τ_{decay} by almost a factor of two in spines (weak depolarization, 1.85 ±

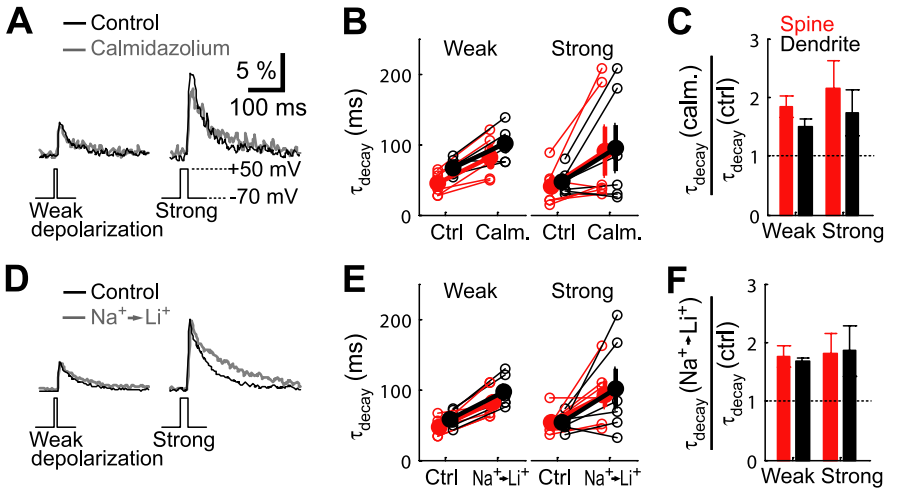

Figure 5. Ca^{2+} extrusion is via PMCA and Na^+/Ca^{2+} exchangers. ***A***, Example of $[Ca^{2+}]$ transients evoked by a weak (left) and strong (right) depolarization in control conditions (black) and calmidazolium (gray). ***B***, τ_{decay} in calmidazolium (Calm.) and control (Ctrl) (open circles, individual cells; filled circles, averages; $n = 6$). ***C***, τ_{decay} in calmidazolium relative to control. ***D***, Example of a $[Ca^{2+}]$ transient evoked by a weak (left) and strong (right) depolarization in control conditions (black) and with Li^+ replacing Na^+ (gray; scale bars as in ***A***). ***E***, $[Ca^{2+}]$ τ_{decay} in Li^+ and control (Ctrl) (open circles, individual cells; filled circles, averages; $n = 6$). ***F***, τ_{decay} in Li^+ normalized to control. Error bars indicate SEM.

0.18; strong depolarization, 2.15 ± 0.46; $n = 6$) and dendrites (weak depolarization, 1.50 ± 0.12; strong depolarization, 1.73 ± 0.40). We obtained similar results when blocking PMCAs with 25–50 μM orthovanadate (supplemental Materials and Methods and supplemental Fig. 4, available at www.jneurosci.org as supplemental material) (Usachev et al., 2002).

Na^+/Ca^{2+} exchange can be inhibited by replacing extracellular Na^+ with ions that are not transported by the exchanger. We recorded $[Ca^{2+}]$ transients evoked by depolarizations before and after replacing Na^+ in the ACSF with Li^+ (Fig. 5*D*) (Mulkey and Zucker, 1992; Koch and Barish, 1994; Fierro et al., 1998). Again, the depolarization pulse width was adjusted to maintain constant $[Ca^{2+}]$ transient amplitudes. Li^+ increased τ_{decay} by almost a factor of 2 (Fig. 5*E*,*F*) (spine: weak depolarization, 1.76 ± 0.18; strong depolarization, 1.81 ± 0.35; dendrite: weak depolarization, 1.67 ± 0.07; strong depolarization, 1.85 ± 0.43; $n = 6$). Changes in resting $[Ca^{2+}]$ after replacing Li^+ for Na^+ were small compared with the amplitudes of depolarization-evoked $[Ca^{2+}]$ transients (relative change in baseline $[Ca^{2+}]$: spine, 14 ± 4%; dendrite, 23 ± 4%; transient amplitude relative to baseline $[Ca^{2+}]$: spine, ≈180%; dendrite, ≈110%; $n = 6$) (supplemental Fig. 3*C*,*D*, available at www.jneurosci.org as supplemental material).

Under our conditions, SERCA pumps do not contribute significantly to Ca^{2+} clearance. The average τ_{decay} in the presence of thapsigargin and ryanodine (spine: weak depolarization, 54.2 ± 7.5 ms; strong depolarization, 58.5 ± 14.5 ms; dendrite: weak depolarization, 58.8 ± 4.3 ms; strong depolarization, 41.5 ± 3.6 ms; $n = 4$; unpaired *t* test; data not shown) was not significantly different from control conditions.

Thus, Na^+/Ca^{2+} exchangers and PMCAs contribute to Ca^{2+} extrusion through the plasma membrane. Because calmidazolium is only a partial blocker of PMCAs (Penniston and Enyedi, 1998), whereas Li^+ completely abolishes Na^+/Ca^{2+} exchanger activity, under our conditions PMCAs likely extrude slightly more than half of Ca^{2+} ions (spines, >46%; dendrites, >33%; $n = 6$) and Na^+/Ca^{2+} exchangers are responsible for extruding most of the remainder (spines, 43%; dendrites, 40%; $n = 6$). Consistent with our physiological measurements, immunofluorescence images revealed that PMCA and Na^+/Ca^{2+} exchangers (NCX2) were expressed in CA1 dendrites and spines (A. Burette and R. Weinberg, personal communication).

Ca^{2+} extrusion via both PMCA and Na^+/Ca^{2+} exchangers depresses

To determine the substrates of Ca^{2+}-dependent depression of Ca^{2+} extrusion, we compared $[Ca^{2+}]$ transients produced by single weak depolarizations and trains (50 Hz) of weak depolarizations, while manipulating Ca^{2+} extrusion mechanisms (Fig. 6). Trains of depolarizations evoked $[Ca^{2+}]$ transients that were similar to those evoked by AP trains. As for APs (Fig. 3*C*), the plateaus of depolarization-evoked transients matched the predicted plateaus calculated based on the $[Ca^{2+}]$ increment per stimulus, stimulus frequency, and τ_{decay} at the end of the train (Eq. 4; supplemental Fig. 2*B*, available at www.jneurosci.org as supplemental material).

Because Na^+/Ca^{2+} exchangers are present in spines and dendrites, depression of extrusion could be mediated in part by the accumulation of cytosolic Na^+, which would reduce the $[Na^+]$ gradient across the plasma membrane and thus the driving force for the exchanger. Consistent with this possibility, in the presence of the Na^+ channel blocker TTX, $[Ca^{2+}]$ transients displayed less pronounced extrusion depression than observed with AP-evoked transients (APs, $n = 17$; depolarization with TTX, $n = 18$) (Fig. 6*A*). This result is consistent with an estimate of the reduction in the forward Ca^{2+} transport rate of the Na^+/Ca^{2+} exchanger based on the change of $[Na^+]$ per AP. An elevation of the internal Na^+ concentration by ~5 mM during a 500-ms-long train of APs at 50 Hz (0.2 mM per AP) (Rose et al., 1999) reduces the Na^+/Ca^{2+} exchanger Ca^{2+} translocation rate by a factor of 0.77 [Regehr (1997), Eq. 2) (with internal $[Ca^{2+}]_i$ of 1 μM, $[Na^+]_i$ of 15 mM, external $[Ca^{2+}]_e$ of 2 mM, $[Na^+]_e$ of 153 mM, $V_m = -70$ mV, and kT = 26.9 mV at 35°C). Thus, depression of extrusion is partially attributable to diminished Ca^{2+} transport by Na^+/Ca^{2+} exchangers caused by accumulation of cytosolic Na^+ during trains of APs.

Why is depression of Ca^{2+} extrusion attributable to cytosolic Na^+ accumulation not observed in the recordings with Fluo-4 (Fig. 2*E*)? Under these conditions, $[Ca^{2+}]$ transients are so small that the Na^+/Ca^{2+} exchangers remain close to equilibrium, implying little net transport of Ca^{2+} ions (Regehr, 1997). When recorded with Fluo-4, the ratios of τ_{decay} for single depolarization-evoked $[Ca^{2+}]$ transients in Li^+ (Na^+/Ca^{2+} exchangers blocked) versus Na^+ were not significantly different from unity (spine, 1.06 ± 0.07; dendrite, 0.96 ± 0.04; $n = 3$; data not shown).

With Na^+/Ca^{2+} exchangers blocked, which Ca^{2+} extrusion mechanism is responsible for the remainder of activity-dependent depression of extrusion? In the presence of extracellular Li^+, $[Ca^{2+}]$ transient decays were slowed dramatically (factor of 4–5) after 50 Hz trains (Fig. 6*B*) compared with single depolarizations (Fig. 6*A*,*C*, right). Under control conditions (Na^+/Ca^{2+} exchangers active), this factor was only ~1.5 (Fig. 6*A*,*C*, left). With Na^+/Ca^{2+} exchangers blocked, the slowing of

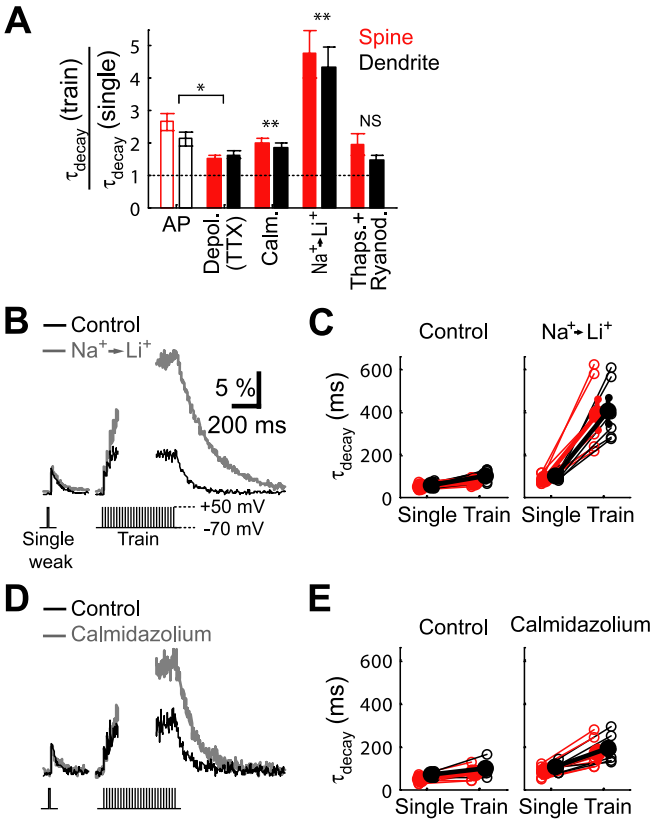

Figure 6. Na^+/Ca^{2+} exchangers and PMCAs are substrates for activity-dependent depression of extrusion. ***A***, τ_{decay} after 50 Hz trains of APs (open bars) or weak depolarization (filled bars) normalized to single stimuli [AP, $n = 17$; depolarization (Depol.), $n = 18$; calmidazolium (Calm.), $n = 6$; Li^+, $n = 6$; thapsigargin plus ryanodine (Thaps. + Ryanod.), $n = 4$; *statistically significant difference, unpaired *t* test; **statistically significant difference compared with internal control; NS, not significant compared with depolarization, unpaired *t* test]. ***B***, $[Ca^{2+}]$ transients evoked by a single (left) and a 50 Hz (right) train of weak depolarizations in control conditions (black) and Li^+ (gray). ***C***, τ_{decay} of $[Ca^{2+}]$ transients (open circles, individual cells; filled circles, averages; $n = 6$). ***D***, $[Ca^{2+}]$ transients evoked by a single (left) and a 50 Hz (right) train of weak depolarizations in control conditions (black) and in calmidazolium (gray; scale bars as in ***B***). ***E***, τ_{decay} of $[Ca^{2+}]$ transients (open circles, individual cells; filled circles, averages; $n = 6$). Error bars indicate SEM.

extrusion caused a dramatic increase in peak $[Ca^{2+}]$ during the train (spine, factor of 3.2 ± 0.4; dendrite, 3.0 ± 0.4; $n = 6$) (Fig. 6*B*). Despite this increase, the enhanced slowing of extrusion was not attributable to saturation of PMCAs (supplemental Fig. 3*E*, available at www.jneurosci.org as supplemental material). Thus, we conclude that PMCAs inactivate in response to intracellular Ca^{2+} accumulations.

With Na^+ accumulations blocked, inactivation of PMCAs seems to mediate the majority of Ca^{2+}-dependent depression of extrusion (Fig. 6*A*,*C*). Partial block of PMCAs with calmidazolium increased τ_{decay} for single depolarizations and the 50 Hz train by a factor of 2 compared with control (spine: single, 1.85 ± 0.15; train, 2.34 ± 0.32; difference not significant; dendrite: single, 1.50 ± 0.12; train, 1.96 ± 0.17; difference significant; $n = 6$) (Fig. 6*E*). Ca^{2+}-dependent depression of extrusion was slightly enhanced in the presence of calmidazolium (spine, 27 ± 15%; dendrite, 33 ± 12%) (Fig. 6*A*). If PMCAs mediate Ca^{2+}-dependent depression of extrusion under these conditions, why is the amplitude of Ca^{2+}-dependent depression of extrusion increased by partial block of PMCAs? By reducing Ca^{2+} extrusion, the presence of calmidazolium leads to larger $[Ca^{2+}]$ accumulations (Fig. 6*D*), which presumably causes stronger inactivation of the remaining PMCAs (for a formal analysis, see supplemental Materials and Methods, available at www.jneurosci.org as supplemental material). However, we cannot exclude an additional contribution of Ca^{2+}-dependent inactivation of Na^+/Ca^{2+} exchangers. Furthermore, this result suggests also that depression of extrusion is not mediated by Ca^{2+}-dependent calmodulin binding to PMCA or one of its regulators, because calmidazolium interferes with calmodulin binding to its targets. However, it is possible that calmodulin is preassociated with PMCAs (Erickson et al., 2001) to control their activity.

In contrast, inhibiting stores with thapsigargin and ryanodine neither prevented nor dramatically increased depression of extrusion (Fig. 6*A*). Thus, uptake into the smooth endoplasmic reticulum did not contribute to depression of Ca^{2+} extrusion, consistent with the finding that it plays only a minor role in extruding Ca^{2+} under our conditions.

Interactions with NMDAR-mediated $[Ca^{2+}]$ signals

To determine whether depression of Ca^{2+} extrusion could play a role in $[Ca^{2+}]$ signals related to synaptic transmission, we combined stimulation of synaptic glutamate receptors by two-photon glutamate uncaging with two-photon $[Ca^{2+}]$ imaging (Carter and Sabatini, 2004; Sobczyk et al., 2005; Losonczy and Magee, 2006) (Fig. 7*A*) (see Materials and Methods). To evoke and isolate currents and Ca^{2+} influx through NMDARs (Fig. 7*E*), experiments were performed in voltage clamp with the Mg^{2+} block relieved (0.1 mM Mg^{2+}), in the presence of the AMPA receptor blocker NBQX, drugs to reduce dendritic excitation and nonlinearities, and drugs to abolish Ca^{2+} release from intracellular stores (see Materials and Methods) (Sobczyk et al., 2005). Uncaging reliably induced NMDAR-mediated uEPSCs and $[Ca^{2+}]$ transients that were primarily restricted to the stimulated spine (Fig. 7*B*). To avoid membrane depolarization and possible activation of VSCCs, the uncaging intensity was limited to keep currents small (mean uEPSC, 9.4 ± 1.1 pA; 14 spines; seven cells).

To test whether NMDAR-mediated Ca^{2+} and Na^+ influx induces depression of Ca^{2+} extrusion, we followed glutamate uncaging with a strong depolarization (interstimulus interval, 250–300 ms). τ_{decay} was significantly larger than under control conditions ($n = 15$ spines) (Fig. 7*C*, red, left, *D*, red). Depression of extrusion was limited to the stimulated spine and did not occur in the parent dendrite (dendritic τ_{decay}; $n = 15$ spines) (Fig. 7*C*, black, right, *D*, black), most likely because the glutamate uncaging-evoked $[Ca^{2+}]$ transients were restricted to single spines (Fig. 7*B*) (Noguchi et al., 2005; Sobczyk et al., 2005). We conclude that NMDAR activation induces depression of extrusion restricted to stimulated spines.

Next we tested how depression of Ca^{2+} extrusion shapes NMDAR-mediated $[Ca^{2+}]$ transients during trains of uncaging stimuli. In the case of NMDAR-mediated $[Ca^{2+}]$ signals in spines, τ_{decay} does not simply reflect extrusion (Eq. 2) but, in addition, is shaped by the time course of the uEPSC and Ca^{2+} diffusion from the spine head into the dendrite. Therefore, to detect differences in the effectiveness of Ca^{2+} extrusion, we compared the integral of $[Ca^{2+}]$ transients normalized to the integral of the NMDAR current ($\Sigma[Ca^{2+}]/\Sigma I_{NMDA}$; see Materials and Methods) (supplemental Eq. S11, available at www.jneurosci.org as supplemental material). The normalization accounts for potential desensitization of NMDAR currents and the resulting reduction in Ca^{2+} influx during trains of uncaging stimuli.

We compared the $[Ca^{2+}]$ transients evoked by a single uncaging stimulus and a train of six uncaging stimuli (10 Hz) (Fig. 7*E*). Surprisingly, on average the normalized $[Ca^{2+}]$ integrals were

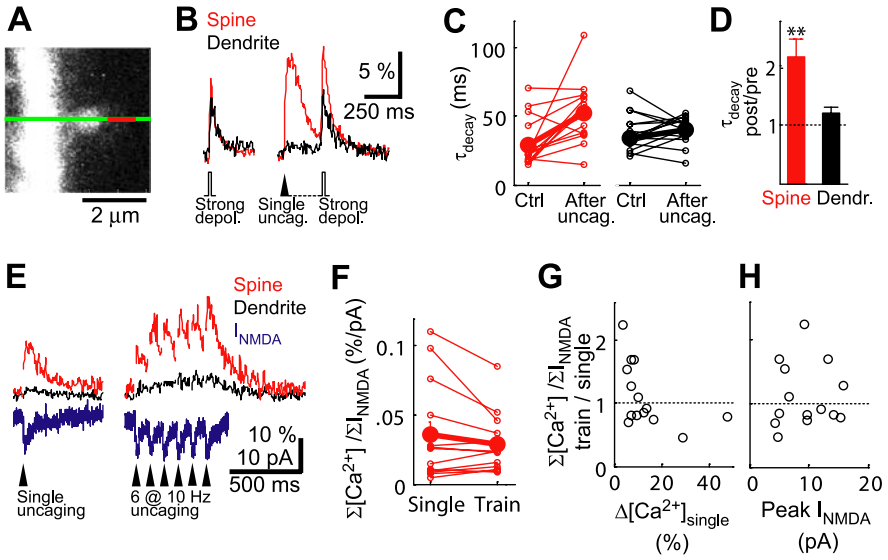

Figure 7. Depression of Ca^{2+} extrusion and Ca^{2+} influx through NMDAR-timing-dependent plasticity of Ca^{2+} extrusion. ***A***, Simultaneous $[Ca^{2+}]$ imaging and glutamate uncaging. The image of a spine is shown. The green line indicates the position of line scans performed for Ca^{2+} imaging. Caged glutamate was photolyzed next to the spine head (red line). ***B***, Examples of $[Ca^{2+}]$ transients evoked by a strong depolarization alone (depol.; left) and glutamate uncaging (uncag.), followed by strong depolarization after 250 ms (right). ***C***, τ_{decay} of $[Ca^{2+}]$ transients evoked by strong depolarization after glutamate uncaging (uncag.) compared with control (Ctrl.; open circles, individual cells; filled circles, averages; $n = 15$ spines, 5 cells). ***D***, Averages and SEM (**statistically significant difference from unity). Dendr., Dendrite. ***E***, $[Ca^{2+}]$ transients (red, spine; black, dendrite) and NMDAR currents (blue) evoked by single glutamate uncaging stimuli (left) and trains of six stimuli at 10 Hz (right) ($n = 14$ spines, 7 cells). ***F***, Glutamate uncaging evoked Ca^{2+} accumulations produced by single stimuli compared with trains of stimuli. Ca^{2+} accumulations were quantified as the integral of $[Ca^{2+}]$ normalized to the integral of NMDAR currents (open circles, individual cells; filled circles, averages; $n = 14$ spines, 7 cells). ***G***, Ca^{2+} accumulation produced by trains of uncaging stimuli normalized to single stimuli as a function of $[Ca^{2+}]$ transient amplitude of the single stimulus response ($\Delta[Ca^{2+}]$). Ca^{2+} accumulations were calculated as in ***F***. ***H***, Ca^{2+} accumulation produced by trains of uncaging stimuli normalized to single stimuli as a function of I_{NMDA} of the single response. Ca^{2+} accumulations were calculated as in ***F***.

not significantly different for single uEPSCs and trains of uEPSCs ($n = 14$ spines) (Fig. 7*F*). Only a subset of spines displayed enhanced $[Ca^{2+}]$ accumulation during trains of uEPSCs. Similarly, trains of depolarization did not significantly change the time course of subsequent NMDAR-mediated $[Ca^{2+}]$ transients ($n = 8$ spines) (supplemental Fig. 5, available at www.jneurosci.org as supplemental material).

Spines have been shown to display heterogeneity in NMDAR-mediated Ca^{2+} signaling in response to glutamate uncaging (Noguchi et al., 2005; Sobczyk et al., 2005). Here we observed that spines also respond to trains of uncaging stimuli in diverse ways. Different spines yielded similar, enhanced, or reduced $[Ca^{2+}]$/NMDAR current integral ratios for trains of uncaging stimuli compared with single stimuli, in which enhancement was preferentially observed if single stimulus-evoked $[Ca^{2+}]$ transients were small [<10% $(G/R)_{max}$] (Fig. 7*G*). A similar correlation was not apparent with respect to the size of the NMDAR-mediated currents (Fig. 7*H*), consistent with the absence of correlation between NMDAR-mediated $[Ca^{2+}]$ transients and currents (Noguchi et al., 2005; Sobczyk et al., 2005).

Discussion

The mechanisms shaping $[Ca^{2+}]$ dynamics in spines and dendrites are critical for Ca^{2+}-dependent signaling in neurons. In contrast to the mechanisms of Ca^{2+} influx and buffering, little is known about Ca^{2+} extrusion and its regulation. We have shown that PMCAs and Na^+/Ca^{2+} exchangers dominate Ca^{2+} clearance from small dendrites and spines in CA1 pyramidal neurons. Extrusion via both PMCAs and Na^+/Ca^{2+} exchangers depresses in an activity-dependent manner, leading to nonlinear Ca^{2+} signaling.

PMCAs and Na^+/Ca^{2+} exchangers extrude Ca^{2+} from dendritic spines

We find that both PMCAs and Na^+/Ca^{2+} exchangers contribute to Ca^{2+} extrusion from spines and dendrites (Fig. 5). PMCAs have been previously detected by immunolocalization in spines from cerebellar Purkinje cells (Stauffer et al., 1997) and hippocampal neurons (DeMarco and Strehler, 2001; Kip et al., 2006). *b* splice variants contain a C-terminal PDZ [postsynaptic density-95 (PSD-95)/Discs large/zona occludens-1]-binding motif, and several PMCA isoforms have been shown to interact with PSD-95 family members at the postsynaptic density (DeMarco and Strehler, 2001; Strehler and Zacharias, 2001).

There are two distinct groups of Na^+/Ca^{2+} exchangers. Members of the NCX family exchange Na^+ and Ca^{2+} ions in a stoichiometric ratio of 3:1, whereas NCKX also exchanges K^+ ions [$4\,Na^+$:($1Ca^{2+} + 1K^+$)] (Blaustein and Lederer, 1999; Lytton et al., 2002). NCX2 labeling is found in apical dendrites and spines of CA1 pyramidal neurons (Burette and Weinberg, personal communication), a finding consistent with studies of NCX2 knock-out mice, which exhibit slowing of Ca^{2+} extrusion in the somato-dendritic compartment (Jeon et al., 2003). Other immunolocalization data suggest that NCX3 can also be found in CA1 dendrites (Canitano et al., 2002; Papa et al., 2003). NCKX can contribute to Ca^{2+} extrusion in the somata of CA1 neurons (Kiedrowski, 2004), but little is known about the subcellular distributions of NCKX.

We found that PMCA and Na^+/Ca^{2+} exchanger together are responsible for the majority of Ca^{2+} clearance from the cytoplasm. Ca^{2+} clearance by uptake into internal stores (endoplasmic reticulum) via SERCA pumps (Mainen et al., 1999; Majewska et al., 2000b; Sabatini et al., 2002) plays only a minor role under our conditions. PMCAs have 10-fold higher affinity and a >10 times lower transport rate than NCX for Ca^{2+} (Blaustein and Lederer, 1999). For this reason, PMCAs have generally been associated with maintaining low resting $[Ca^{2+}]$ and NCX with rapid clearance of $[Ca^{2+}]$ transients (Thayer et al., 2002). In contrast with this view, under our experimental conditions, PMCA and Na^+/Ca^{2+} exchanger contribute to extrusion of Ca^{2+} to similar extents. It is possible that Na^+/Ca^{2+} exchanger dominates Ca^{2+} clearance for larger $[Ca^{2+}]$ transients than those probed in our study.

Activity- and Ca^{2+}-dependent depression of Ca^{2+} extrusion

Large and prolonged $[Ca^{2+}]$ transients, for example those evoked by trains of APs relevant for hippocampal function (Czurko et al., 1999), decay more slowly than transients evoked by single APs. This positive feedback is attributable to Ca^{2+}-dependent depression of extrusion. Previous measurements of AP-evoked $[Ca^{2+}]$ signals used high-affinity indicators with

higher added buffer capacity, and thus much less (Helmchen et al., 1996) or no (Maravall et al., 2000) activity-dependent depression of extrusion was detected. Depression of extrusion after AP trains was reported in one study using high-affinity buffer (Callaway and Ross, 1995). However, because the indicator was loaded through a sharp electrode, it is possible that the indicator concentration in the dendrite was sufficiently low so that it corresponded to our standard low added buffer capacity condition.

We found that with Na^+ channels blocked, activity-dependent depression of extrusion was reduced. The most straightforward interpretation of our data are that Na^+ accumulation during trains of APs reduces the driving force for Na^+/Ca^{2+} exchangers (Blaustein and Lederer, 1999; Thayer et al., 2002). A similar interplay between Na^+ accumulation and Ca^{2+} extrusion has been studied in presynaptic terminals (Mulkey and Zucker, 1992; Regehr, 1997). The Na^+-dependent depression was not observed under the condition of high Ca^{2+} buffering because for the tiny $[Ca^{2+}]$ levels achieved under these conditions, Na^+/Ca^{2+} exchangers remained close to equilibrium and contributed effectively no net ion translocation to total extrusion.

With Na^+/Ca^{2+} exchangers blocked, we observed very large $[Ca^{2+}]$ accumulations and a more pronounced activity-dependent depression of extrusion (Fig. 6), reflecting Ca^{2+}-dependent inactivation of PMCAs. Although $[Ca^{2+}]$ reached up to 2 μM, we found no indication of PMCA saturation (supplemental Fig. 3*E*, available at www.jneurosci.org as supplemental material). In contrast, biochemical data reports Ca^{2+} affinities in the range ~0.1–1.0 μM with calmodulin bound (~20 μM without calmodulin) and affinities for calmodulin on the order of ~1 nM (Carafoli, 1992; Caride et al., 2001). Because the concentration of calmodulin ranges from 10 to 100 μM (Xia and Storm, 2005), PMCAs would be expected to be predominantly in the high-affinity state and thus saturated under our conditions. Absence of saturation argues instead that PMCAs have surprisingly low affinity for Ca^{2+} in intact neurons, at least in their inactivated state (Strehler and Zacharias, 2001).

Ca^{2+}-dependent inactivation of PMCAs resembles Ca^{2+}-dependent inactivation of VSCCs (Budde et al., 2002). Although various signaling pathways have the potential to modulate PMCA activity (Strehler and Zacharias, 2001; Thayer et al., 2002), the mechanisms underlying the observed Ca^{2+}-dependent inactivation remain uncertain.

Depression of Ca^{2+} extrusion and synaptic $[Ca^{2+}]$ signaling

Activation of synaptic NMDARs by glutamate uncaging produced depression of extrusion in the stimulated spine. This is not surprising, because under our experimental conditions, NMDAR activation produces larger accumulations of Na^+ and Ca^{2+} in the stimulated spine than do trains of APs (Rose and Konnerth, 2001; Sabatini et al., 2002). We also expected to observe the reverse, an enhanced accumulation of Ca^{2+} attributable to slowing of extrusion during trains of NMDAR-mediated $[Ca^{2+}]$ transients. Surprisingly, $[Ca^{2+}]$ per stimulus was similar for single uncaging stimuli and trains. However, there was heterogeneity in the NMDAR-mediated $[Ca^{2+}]$ response of individual spines to trains of uncaging stimuli. Some spines showed an enhanced $[Ca^{2+}]$ per stimulus during trains as expected when depression of Ca^{2+} extrusion occurs, whereas other spines behaved in opposite ways (Fig. 7*G*). This heterogeneity in Ca^{2+} handling may be interesting with respect to the induction of synaptic plasticity. It could reflect input-specific Ca^{2+} handling in spines, or different functional states arising from metaplasticity.

In the spines that did not produce enhanced Ca^{2+} accumulations during trains of uncaging stimuli, depression of Ca^{2+} extrusion might be compensated for or obscured by one of the following mechanisms. (1) The activity of particular extrusion mechanisms could be selectively enhanced. Because, for example, PMCA *b* splice variants interact with PSD-95 family members at the postsynaptic density (DeMarco and Strehler, 2001; Strehler and Zacharias, 2001), different Na^+/Ca^{2+} exchanger and PMCA isoforms are potentially regulated in diverse ways and associated with different postsynaptic signaling complexes. (2) The amount of Ca^{2+} influx could decrease without a change in the NMDAR current. NMDAR currents display short-term plasticity (Tong et al., 1995), which might extend to Ca^{2+} permeability, because there is evidence that the Ca^{2+} permeability of NMDAR can be selectively regulated (Sobczyk et al., 2005). (3) Ca^{2+} clearance could be dominated by diffusion into the dendrite across the spine neck (Majewska et al., 2000a; Bloodgood and Sabatini, 2005). Future experiments will have to address these possibilities.

Functional physiological role of depression of Ca^{2+} extrusion

$[Ca^{2+}]$ signals in dendritic spines play a key role in inducing diverse forms of neuronal plasticity, including long-term depression and potentiation. Stimuli that produce an enhancement of synaptic strength are associated with higher-amplitude $[Ca^{2+}]$ signals compared with stimuli that lead to a decrease in synaptic strength (Cummings et al., 1996; Yang et al., 1999; Froemke et al., 2005). Our results show that the rate of Ca^{2+} extrusion, which determines the temporal summation of $[Ca^{2+}]$ signals, is regulated in an activity- and Ca^{2+}-dependent manner. This positive feedback mechanism causes nonlinear Ca^{2+} signaling. Therefore, it can contribute to translating differences in stimuli into differential activation of Ca^{2+}-dependent signaling cascades to induce different forms of plasticity.

We show that the clearance of VSCC-mediated $[Ca^{2+}]$ transient is slowed subsequent to NMDAR activation, but not vice versa. The order of the stimuli can thus play an important role in determining the total integrated Ca^{2+} accumulation in individual dendritic spines. This is reminiscent of STDP, in which postsynaptic spiking before synaptic activation leads to synaptic depression, whereas postsynaptic spiking after synaptic activation results in synaptic potentiation (Sjostrom and Nelson, 2002). Depression of extrusion might play a role in the induction of plasticity by producing larger integrated Ca^{2+} accumulations if synaptic stimuli precede postsynaptic spiking. However, the recovery time constant of depression of extrusion is slower than the time window for STDP (500 ms vs 10–50 ms). It is possible that depression of extrusion plays a role in learning rules that involve longer time scales (Larson and Lynch, 1986).

The heterogeneity in Ca^{2+} handling after trains of NMDAR activations, where spines displayed either an unchanged or enhanced accumulation of $[Ca^{2+}]$ compared with a single stimulus, could be a mechanisms underlying synaptic metaplasticity (Fusi et al., 2005). For example, a potentiated spine might not express depression of extrusion and therefore would be less likely to be potentiated further. Conversely, depressed spines would express depression of extrusion and be more likely to be potentiated by generating enhanced $[Ca^{2+}]$ accumulations during trains of synaptic activation.

References

Blaustein MP, Lederer WJ (1999) Sodium/calcium exchange: its physiological implications. Physiol Rev 79:763–854.

Bloodgood BL, Sabatini BL (2005) Neuronal activity regulates diffusion across the neck of dendritic spines. Science 310:866–869.

Budde T, Meuth S, Pape HC (2002) Calcium-dependent inactivation of neuronal calcium channels. Nat Rev Neurosci 3:873–883.

Callaway JC, Ross WN (1995) Frequency-dependent propagation of sodium action potentials in dendrites of hippocampal CA1 pyramidal neurons. J Neurophysiol 74:1395–1403.

Canitano A, Papa M, Boscia F, Castaldo P, Sellitti S, Taglialatela M, Annunziato L (2002) Brain distribution of the Na^+/Ca^{2+} exchanger-encoding genes NCX1, NCX2, and NCX3 and their related proteins in the central nervous system. Ann NY Acad Sci 976:394–404.

Carafoli E (1992) The Ca^{2+} pump of the plasma membrane. J Biol Chem 267:2115–2118.

Caride AJ, Filoteo AG, Penheiter AR, Paszty K, Enyedi A, Penniston JT (2001) Delayed activation of the plasma membrane calcium pump by a sudden increase in Ca^{2+}: fast pumps reside in fast cells. Cell Calcium 30:49–57.

Carter AG, Sabatini BL (2004) State-dependent calcium signaling in dendritic spines of striatal medium spiny neurons. Neuron 44:483–493.

Cummings JA, Mulkey RM, Nicoll RA, Malenka RC (1996) Ca^{2+} signaling requirements for long-term depression in the hippocampus. Neuron 16:825–833.

Czurko A, Hirase H, Csicsvari J, Buzsaki G (1999) Sustained activation of hippocampal pyramidal cells by "space clamping" in a running wheel. Eur J Neurosci 11:344–352.

DeMarco SJ, Strehler EE (2001) Plasma membrane Ca2+-atpase isoforms 2b and 4b interact promiscuously and selectively with members of the membrane-associated guanylate kinase family of PDZ (PSD95/Dlg/ZO-1) domain-containing proteins. J Biol Chem 276:21594–21600.

Emptage N, Bliss TVP, Fine A (1999) Single synaptic events evoke NMDA receptor-mediated release of calcium from internal stores in hippocampal dendritic spines. Neuron 22:115–124.

Erickson MG, Alseikhan BA, Peterson BZ, Yue DT (2001) Preassociation of calmodulin with voltage-gated Ca^{2+} channels revealed by fret in single living cells. Neuron 31:973–985.

Fierro L, DiPolo R, Llano I (1998) Intracellular calcium clearance in Purkinje cell somata from rat cerebellar slices. J Physiol (Lond) 510:499–512.

Froemke RC, Poo MM, Dan Y (2005) Spike-timing-dependent synaptic plasticity depends on dendritic location. Nature 434:221–225.

Fusi S, Drew PJ, Abbott LF (2005) Cascade models of synaptically stored memories. Neuron 45:599–611.

Garaschuk O, Yaari Y, Konnerth A (1997) Release and sequestration of calcium by ryanodine-sensitive stores in rat hippocampal neurones. J Physiol (Lond) 502:13–30.

Harris KM, Stevens JK (1989) Dendritic spines of CA1 pyramidal cells in the rat hippocampus: serial electron microscopy with reference to their biophysical characteristics. J Neurosci 9:2982–2997.

Helmchen F, Imoto K, Sakmann B (1996) Ca^{2+} buffering and action potential-evoked Ca^{2+} signaling in dendrites of pyramidal neurons. Biophys J 70:1069–1081.

Jacobs JM, Meyer T (1997) Control of action potential-induced Ca^{2+} signaling in the soma of hippocampal neurons by Ca^{2+} release from intracellular stores. J Neurosci 17:4129–4135.

Jeon D, Yang YM, Jeong MJ, Philipson KD, Rhim H, Shin HS (2003) Enhanced learning and memory in mice lacking Na^+/Ca^{2+} exchanger 2. Neuron 38:965–976.

Kaczorowski GJ, Slaughter RS, King VF, Garcia ML (1989) Inhibitors of sodium-calcium exchange: identification and development of probes of transport activity. Biochim Biophys Acta 988:287–302.

Kennedy MB (2000) Signal-processing machines at the postsynaptic density. Science 290:750–754.

Kiedrowski L (2004) High activity of K^+-dependent plasmalemmal Na^+/Ca^{2+} exchangers in hippocampal CA1 neurons. NeuroReport 15:2113–2116.

Kip SN, Gray NW, Burette A, Canbay A, Weinberg RJ, Strehler EE (2006) Changes in the expression of plasma membrane calcium extrusion systems during the maturation of hippocampal neurons. Hippocampus 16:20–34.

Koch RA, Barish ME (1994) Perturbation of intracellular calcium and hydrogen ion regulation in cultured mouse hippocampal neurons by reduction of the sodium ion concentration gradient. J Neurosci 14:2585–2593.

Koester HJ, Sakmann B (1998) Calcium dynamics in single spines during coincident pre- and postsynaptic activity depend on relative timing of back-propagating action potentials and subthreshold excitatory postsynaptic potentials. Proc Natl Acad Sci USA 95:9596–9601.

Kovalchuk Y, Eilers J, Lisman J, Konnerth A (2000) NMDA receptor-mediated subthreshold Ca^{2+} signals in spines of hippocampal neurons. J Neurosci 20:1791–1799.

Larson J, Lynch G (1986) Induction of synaptic potentiation in hippocampus by patterned stimulation involves two events. Science 232:985–988.

Lee S-H, Rosenmund C, Schwaller B, Neher E (2000) Differences in Ca^{2+} buffering properties between excitatory and inhibitory hippocampal neurons from the rat. J Physiol (Lond) 525:405–418.

Losonczy A, Magee JC (2006) Integrative properties of radial oblique dendrites in hippocampal CA1 pyramidal neurons. Neuron 50:291–307.

Lytton J, Li XF, Dong H, Kraev A (2002) K+-dependent Na^+/Ca^{2+} exchangers in the brain. Ann NY Acad Sci 976:382–393.

Mainen ZF, Malinow R, Svoboda K (1999) Synaptic calcium transients in single spines indicate that NMDA receptors are not saturated. Nature 399:151–155.

Majewska A, Brown E, Ross J, Yuste R (2000a) Mechanisms of calcium decay kinetics in hippocampal spines: role of spine calcium pumps and calcium diffusion through the spine neck in biochemical compartmentalization. J Neurosci 20:1722–1734.

Majewska A, Tashiro A, Yuste R (2000b) Regulation of spine calcium dynamics by rapid spine motility. J Neurosci 20:8262–8268.

Maravall M, Mainen ZM, Sabatini BL, Svoboda K (2000) Estimating intracellular calcium concentrations and buffering without wavelength ratioing. Biophys J 78:2655–2667.

Markram H, Helm PJ, Sakmann B (1995) Dendritic calcium transients evoked by single back-propagating action potentials in rat neocortical pyramidal neurons. J Physiol (Lond) 485:1–20.

Mulkey RM, Zucker RS (1992) Posttetanic potentiation at the crayfish neuromuscular junction is dependent on both intracellular calcium and sodium ion accumulation. J Neurosci 12:4327–4336.

Muller W, Connor JA (1991) Dendritic spines as individual neuronal compartments for synaptic Ca^{2+} responses. Nature 354:73–76.

Murphy TH, Baraban JM, Wier WG, Blatter LA (1994) Visualization of quantal synaptic transmission by dendritic calcium imaging. Science 263:529–532.

Neher E, Augustine GJ (1992) Calcium gradients and buffers in bovine chromaffin cells. J Physiol (Lond) 450:273–301.

Nimchinsky EA, Sabatini BL, Svoboda K (2002) Structure and function of dendritic spines. Annu Rev Physiol 64:313–353.

Noguchi J, Matsuzaki M, Ellis-Davies GC, Kasai H (2005) Spine-neck geometry determines NMDA receptor-dependent Ca^{2+} signaling in dendrites. Neuron 46:609–622.

Papa M, Canitano A, Boscia F, Castaldo P, Sellitti S, Porzig H, Taglialatela M, Annunziato L (2003) Differential expression of the Na^+-Ca^{2+} exchanger transcripts and proteins in rat brain regions. J Comp Neurol 461:31–48.

Penniston JT, Enyedi A (1998) Modulation of the plasma membrane Ca^{2+} pump. J Membr Biol 165:101–109.

Pologruto TA, Sabatini BL, Svoboda K (2003) ScanImage: flexible software for operating laser-scanning microscopes. BioMed Eng OnLine 2:13.

Regehr WG (1997) Interplay between sodium and calcium dynamics in granule cell presynaptic terminals. Biophys J 73:2476–2488.

Regehr WG, Atluri PP (1995) Calcium transients in cerebellar granule cell presynaptic terminals. Biophys J 68:2156–2170.

Rose CR, Konnerth A (2001) NMDA receptor-mediated Na^+ signals in spines and dendrites. J Neurosci 21:4207–4214.

Rose CR, Kovalchuk Y, Eilers J, Konnerth A (1999) Two-photon Na^+ imaging in spines and fine dendrites of central neurons. Pflügers Arch 439:201–207.

Sabatini BL, Svoboda K (2000) Analysis of calcium channels in single spines using optical fluctuation analysis. Nature 408:589–593.

Sabatini BL, Maravall M, Svoboda K (2001) Ca^{2+} signaling in dendritic spines. Curr Opin Neurobiol 11:349–356.

Sabatini BS, Oertner TG, Svoboda K (2002) The life-cycle of Ca^{2+} ions in spines. Neuron 33:439–452.

Sandler VM, Barbara JG (1999) Calcium-induced calcium release contributes to action potential-evoked calcium transients in hippocampal CA1 pyramidal neurons. J Neurosci 19:4325–4336.

Schiller J, Schiller Y, Clapham DE (1998) Amplification of calcium influx into dendritic spines during associative pre- and postsynaptic activation:

the role of direct calcium influx through the NMDA receptor. Nat Neurosci 1:114–118.

Sjostrom PJ, Nelson SB (2002) Spike timing, calcium signals and synaptic plasticity. Curr Opin Neurobiol 12:305–314.

Sobczyk A, Scheuss V, Svoboda K (2005) NMDA receptor subunit-dependent $[Ca^{2+}]$ signaling in individual hippocampal dendritic spines. J Neurosci 25:6037–6046.

Stauffer TP, Guerini D, Celio MR, Carafoli E (1997) Immunolocalization of the plasma membrane Ca^{2+} pump isoforms in the rat brain. Brain Res 748:21–29.

Strehler EE, Zacharias DA (2001) Role of alternative splicing in generating isoform diversity among plasma membrane calcium pumps. Physiol Rev 81:21–50.

Svoboda K, Tank DW, Denk W (1996) Direct measurement of coupling between dendritic spines and shafts. Science 272:716–719.

Tank DW, Regehr WG, Delaney KR (1995) A quantitative analysis of presynaptic calcium dynamics that contribute to short term enhancement. J Neurosci 15:7940–7952.

Thayer SA, Usachev YM, Pottorf WJ (2002) Modulating Ca^{2+} clearance from neurons. Front Biosci 7:d1255–d1279.

Tong G, Shepherd D, Jahr CE (1995) Synaptic desensitization of NMDA receptors by calcineurin. Science 267:1510–1512.

Usachev YM, DeMarco SJ, Campbell C, Strehler EE, Thayer SA (2002) Bradykinin and ATP accelerate Ca^{2+} efflux from rat sensory neurons via protein kinase C and the plasma membrane Ca^{2+} pump isoform 4. Neuron 33:113–122.

Werth JL, Usachev YM, Thayer SA (1996) Modulation of calcium efflux from cultured rat dorsal root ganglion neurons. J Neurosci 16:1008–1015.

Xia Z, Storm DR (2005) The role of calmodulin as a signal integrator for synaptic plasticity. Nat Rev Neurosci 6:267–276.

Yang SN, Tang YG, Zucker RS (1999) Selective induction of LTP and LTD by postsynaptic $[Ca^{2+}]_i$ elevation. J Neurophysiol 81:781–787.

Yasuda R, Sabatini BL, Svoboda K (2003) Plasticity of calcium channels in dendritic spines. Nat Neurosci 6:948–955.

Yasuda R, Nimchinsky EA, Scheuss V, Pologruto TA, Oertner TG, Sabatini BL, Svoboda K (2004) Imaging calcium concentration dynamics in small neuronal compartments. Sci STKE 2004:pl5.

Yuste R, Denk W (1995) Dendritic spines as basic functional units of neuronal integration. Nature 375:682–684.